

Lithofacies-dependent rock-physics templates of an unconventional shale reservoir on the North Slope, Alaska

Minh Tran¹, Tapan Mukerji², and Allegra Hosford Scheirer²

Abstract

Over the past 20 years, oil and gas companies have turned their attention to producing petroleum directly from organic-rich shale. Successful exploration, appraisal, and production strategies for source rocks critically depend on reliable identification of their organic components (kerogen, in particular) and their generation potential. There is mounting demand to evaluate organic richness in terms of quantity (i.e., total organic carbon) and quality (i.e., hydrogen index) from seismic data, which is usually the only source of information in the early development period of emerging shale plays. We have delineated major seismic lithofacies on the Alaska North Slope using elastic, seismic, and petrophysical properties. We performed a well-established quantitative seismic interpretation workflow to integrate geochemical data in the lithofacies definition. Rock-physics templates (RPTs) of seismic parameters, acoustic impedance, versus P-wave to S-wave velocity ratio (V_P/V_S), are constructed for each lithofacies to assess variations in pore fluid and lithology. We developed correlations between source rock properties (hydrogen index and total organic carbon) and petrophysical properties (bulk density, porosity, and sonic velocity ratio) of the major lithofacies. These correlations, together with facies-specific RPTs, can be used to predict organic richness and source rock properties away from drilled wells. The models are validated by training data from two regional wells to observe their applicability on the Alaska North Slope.

Introduction

The Alaska North Slope (officially the Colville Basin) is estimated to contain approximately 40% of the total undiscovered, technically recoverable oil and natural gas resources in the United States, with more than 30 billion barrels of oil and nearly 200 trillion cubic feet of natural gas (Bird, 2001). Shale oil exploration has gained traction over the past 20 years because of the development and maturation of technologies such as horizontal drilling and hydraulic fracturing, but it has not yet been established in Alaska. Historically, petroleum exploration and production on the Alaska North Slope have been concentrated along the coast of the Beaufort Sea, which approximates the buried hinge line of the Barrow Arch (the dashed line in Figure 1). Unfortunately, relatively few wells have been drilled outside of the producing fields. This dearth of wells renders difficult the determination of geologic and engineering parameters necessary to evaluate organic-rich source rocks for unconventional potential. For example, the lack of geomechanical and regional stress direction data hinders the attempt to successfully perform hydraulic fracturing, which deters commercial development of Alaska North Slope unconventional plays. Further, due to the complex lithology as well as organic and petrophysical hetero-

geneity in shale and mudrocks, prospecting for resource plays is challenging in sparsely drilled areas such as the central North Slope. Thus, a key component of studying the unconventional potential of the North Slope is to robustly predict lithologic, organic, and petrophysical variations where well penetrations are lacking.

This study characterizes the petrophysical, geochemical, and elastic properties of shale lithofacies in the subsurface of the Alaska North Slope downdip (south) of the producing fields, thus laying the groundwork for a reliable classification data set (P-wave velocity, S-wave velocity, and bulk density). A seismic lithofacies is defined as a set of geologic and sedimentological features that span a similar range of seismic and petrophysical properties (Avseth et al., 2005). Sharing characteristic sedimentologic and rock-physics signatures, a seismic lithofacies governs the quantitative interpretation of seismic data for reservoir geometry and porosity. Besides, elastic properties are used to evaluate the geomechanical stability of the formation and optimal drilling direction during appraisal, development, and enhanced oil recovery (Temizel et al., 2016; Tran et al., 2018; Tran and Jha, 2020).

For this study, geochemical data are incorporated into the lithofacies definition because they enhance

¹University of Southern California, Los Angeles, California, USA. E-mail: tranmt@usc.edu (corresponding author).

²Stanford University, Stanford, California, USA. E-mail: mukerji@stanford.edu; allegras@stanford.edu.

Manuscript received by the Editor 13 August 2019; revised manuscript received 17 February 2020; published ahead of production 11 June 2020; published online 15 June 2020. This paper appears in *Interpretation*, Vol. 8, No. 3 (August 2020); p. T611–T623, 14 FIGS., 2 TABLES.

<http://dx.doi.org/10.1190/INT-2019-0156.1>. © 2020 Society of Exploration Geophysicists and American Association of Petroleum Geologists. All rights reserved.

the organic characterization of source rocks and support logging data calibration (Bhattacharya and Timothy, 2019). Generally, shale heterogeneity is best documented with conventional and sidewall cores, but coring is typically limited spatially across a basin and is expensive to obtain and analyze (Gupta et al., 2013). In contrast to the sparsity of cored material, well logs are acquired in nearly each drilled exploration well, thereby filling gaps in subsurface characterization in which cored material is lacking. A further advantage of well logs is their dense vertical resolution — typically 0.5 ft (0.15 m) — over most of the rock section penetrated by the well. Neither the conventional nor sidewall core typically spans the entire well path. Thus, log data augment and complement cored geologic units for classification and will be used extensively in this study.

Recent attempts to characterize shale lithofacies focus on data-driven techniques such as the self-consistent approximation and unsupervised neural networks (Saneifar et al., 2015). Understanding the distributions of elastic properties (P- and S-wave velocities and bulk density) within and across different seismic lithofacies is an important step in the statistical rock-physics workflow. There is a need to account for different physical and geologic scenarios expected across the prospective exploration area but that might not be present at the wells. A possible solution is to use rock-physics-guided correlated Monte Carlo simulations to expand the training data set to account for natural variability. Substantially,

more core analyses also will improve the quality of the training data set and thus add value for more reliable correlations. To facilitate the statistical classification step of the quantitative seismic interpretation (QSI) workflow, we need to ensure that the essence of log-derived data is reliable. In this study, cross-validation and calibration of log-derived properties with core data are performed to characterize major shale lithofacies. We first review the geologic setting of the study area followed by a description of the available data set and how it is used to define seismic lithofacies. The construction of the rock-physics template (RPT) then describes how rock physics effective medium models are calibrated with data. Finally, we conclude with the applicability of the RPTs for QSI.

Geologic setting

Several source rock units have been identified as sources of petroleum in the subsurface of the Alaska North Slope (Bird, 1994; Magoon et al., 2003; Peters et al., 2008, among many others). These are, from youngest to oldest (i.e., well penetration order), the Hue Shale, its basal highly radioactive zone ([HRZ], also called the gamma-ray zone [GRZ]), the pebble shale unit (formally the Kalubik Formation), the Kingak Shale (specifically the basal organic-rich interval), and the Shublik Formation (Figure 2). The most relevant geologic features, depositional history, and source rock characteristics of each lithofacies are discussed here.

Shublik Formation

Being the primary source rock of petroleum in the North Slope (Magoon and Bird, 1985; Bird, 2001; Peters et al., 2008), the Triassic Shublik Formation was deposited in a shelfal marine environment, and it caps the Ellesmerian megasequence (Figure 2). The formation is a regionally extensive mudstone of variable lithology, including phosphatic facies, shale, siltstone, and carbonate (Parrish, 1987; Kupecz, 1995; Bird, 2001; Yurchenko et al., 2018). Much of the Shublik Formation is carbonate rich (Figure 3), but dense accessory minerals such as pyrite likely have a significant effect on the density logs. The total organic carbon (TOC) of the Shublik Formation ranges from 0.5 to 13.1 wt% in the Phoenix-1 well (Robison et al., 1996), which is located offshore. The original petroleum potential of the Shublik as indicated by the hydrogen index is similarly variable, but the kerogen type is dominantly oil-prone types I and II (Robison et al., 1996; Peters et al., 2006).

Kingak Shale

The Jurassic-Lower Cretaceous Kingak Shale immediately overlies the

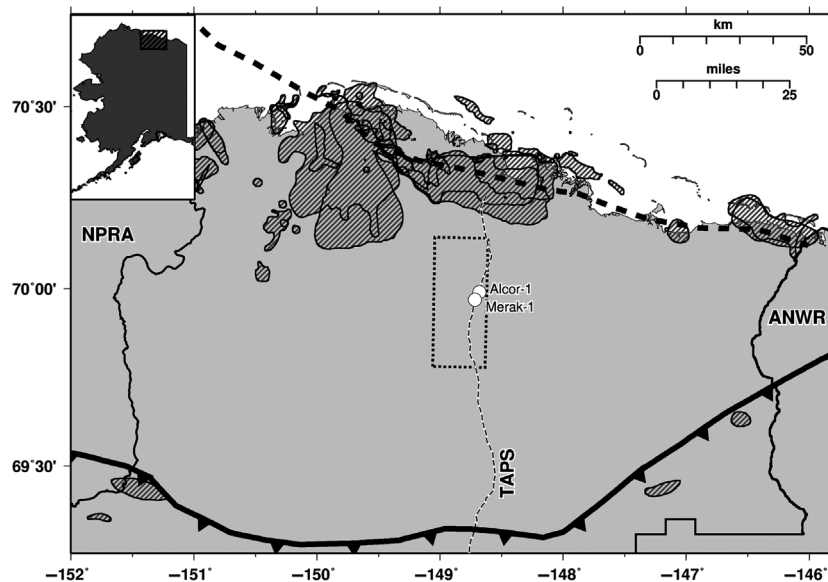


Figure 1. Location map of the Central North Slope, defined as the area between the National Petroleum Reserve Alaska (NPRA), the Alaska National Wildlife Refuge (ANWR), the foothills of the Brooks Range (the thrust front symbols), and the hinge line of the buried Barrow Arch (the heavy dashed line) and the Beaufort Sea coast. The oil and gas fields are shown by the hatched polygons; virtually all fields in the north, along the coast, are producing, whereas those shown to the south are nonproducing (gas). The dashed line (TAPS) is the Trans-Alaska Pipeline System. The dotted rectangle marks the perimeter of the 3D seismic survey from which data are used in this study. Well data come from Alcor-1 and Merak-1 (the open circles). Coordinates use the NAD83 datum.

Shublik Formation (except where the relatively thin Sag River Sandstone intervenes in the producing fields) and is the basal interval of the Beaufortian megasequence (Figure 2). It was deposited during a rift event that today is marked by the buried Barrow Arch (Magoon and Claypool, 1984; Hubbard et al., 1987) (Figure 1) and is characterized by dark-gray shale (Magoon and Claypool, 1984). Although the Kingak Shale is in places thousands of feet thick, the organic-rich interval lies at its base. Marine and terrigenous organic matter are found in this interval, where the total carbon content ranges from 0.94 to 6.3 wt% in 27 well penetrations (Peters et al., 2006). The Lower Cretaceous Unconformity, created by sequences of uplift and erosion events of the rift margin, beveled the top of the Kingak Shale near the coastline. This event probably induced enhanced porosity in subunconformity reservoirs and provided a migration pathway to the largest oilfields on the Alaska North Slope (Bird, 2001).

Pebble shale unit

The pebble shale unit, the uppermost interval of the Beaufortian megasequence, is characterized by pebbles and rounded grains embedded in a shale matrix as well as clay-rich mudstone with local silt and pyrite (Keller and Macquaker, 2001). The kerogen type varies regionally from oil-prone in the west to gas-prone in the east (Molenaar et al., 1987; Keller and Macquaker, 2001). Despite the “good” to “excellent” quantities of TOC (in the classification system of Peters and Cassa, 1994) — 1.5–4.4 wt% in 28 well penetrations — crude oil that is genetically linked to the pebble shale unit has never been found.

Hue Shale and HRZ

Deposition of the Hue Shale and its basal HRZ mark the beginning of the Brookian megasequence at approximately 120 Ma (Figure 2) when siliciclastic sediment from older orogenic events shed into the basin from west to east. Facies of the Hue Shale indicate deposition in a deepwater basin plain environment (Keller and Macquaker, 2001). Because of the west-to-east deposition of the Hue Shale, the unit thickens eastward, thereby diluting organic content with clastic sediments. The upper part of the Hue Shale thus has lower organic quality (HI) and quantity (TOC) relative to the HRZ. As expected, the HRZ is distinguished based on its high gamma-ray magnitude [often >200 API (American Petroleum Institute)]. It is a condensed distal shale. Organic carbon in the Hue-HRZ interval ranges from 1.3 to 5.5 wt% in 33 wellbores (Peters et al., 2006).

A ternary diagram commonly used for classifying mudrocks characterizes the lithologic components of North Slope organic-rich shales in the context of established North American shale plays. In this scheme, shale is divided into three major classes depending on the variation in lithology: argillaceous shale (rich in clay minerals), calcareous shale (rich in calcite and dolomite), and siliceous shale (rich in biogenic and detrital quartz/feldspar). The mineralogy of North Slope shales shown on

Figure 3 derives from X-ray powder diffraction (XRD) data on core samples from Alcor-1 and Merak-1 with the data normalized to 1 after discarding accessory minerals. Figure 3 shows that the clay content of the upper three organic-rich shales strictly increases with drill depth; the Hue Shale comprises 30%–40% clay, the HRZ contains 45%–55% clay, and the Kingak Shale is the richest in clay with 65% to nearly 80%. Moreover, these three source rocks contain no carbonate at all. In contrast, most samples from the Shublik Formation in the two wells have approximately 80% limestone and nearly no clay (Figure 3).

Methodology

In this study, regional geology, standard triple-combo logging suites, and petrophysical and geochemical analyses of core plugs are critical inputs to obtain

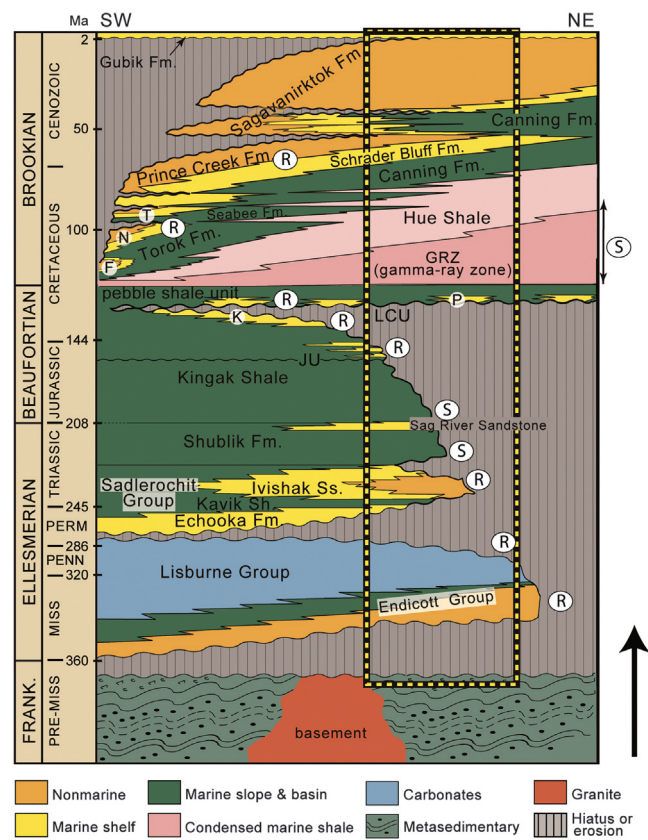


Figure 2. Generalized chronostratigraphy of the Prudhoe Bay field area (inside the dashed box) relative to that of the regional onshore Alaska North Slope. Tectonostratigraphic sequences are in capital letters on the left. Oil-prone source rocks discussed in this paper are indicated by the circled S, and important reservoir rocks are indicated by the circled R. The age span of Hue-GRZ is updated and based on Lease et al. (2018). F, Fortress Mountain Formation; GRZ, gamma-ray zone (this is the same as HRZ, highly radioactive zone; both usages appear in the literature); JU, Jurassic unconformity; K, Kuparuk River Sandstone; LCU, Lower Cretaceous Unconformity; N, Nanushuk Formation; P, Put River Sandstone; and T, Tuluvak Formation. The figure is modified from Houseknecht and Bird (2006).

basic facies definition, which is the first step of a more comprehensive statistical rock physics evaluation workflow (Figure 4). QSI demonstrates how rock physics can be applied to predict reservoir parameters such as lithology, pore fluid, and source rock character from seismically derived attributes (Figure 4). Based on available logs, cores, and Alaska North Slope regional geology, we identify major seismic lithofacies based on the multivariate distribution of different properties. Rock physics aids in relating elastic properties and seismic signatures to petrophysical properties. Geochemical parameters are integrated into the workflow by establishing correlations between elastic and source rock properties. After calibrating inverted seismic data in the area of interest, this data set can be used as an input for classifying lithology and source rock character to detect sweet spots of organic-rich source rock for development.

In this study, we focus on the parts of the workflow that are related to constructing a reliable elastic and geochemical training data set of each geologically defined lithofacies. This captures their multivariate distribution of properties. Well log data (density, gamma ray, resistivity, and sonic wave velocities) are extracted for exploratory data analysis. The use of crossplots between relevant log-derived properties to separate lithofacies is a fast and simple process that also can be applied at the well site. We also use a qualitative assessment routine to evaluate and screen certain criteria while performing exploratory data analysis; for example, the neutron log cannot be used in radioactive shale intervals because cross-validation shows high values of neutron porosity relative to core values. Based on the top and base depths of different lithofacies in the well, we delineate and build a log-based training data set of each shale facies. Preliminary quality checks are performed to remove anomalous log readings due to equip-

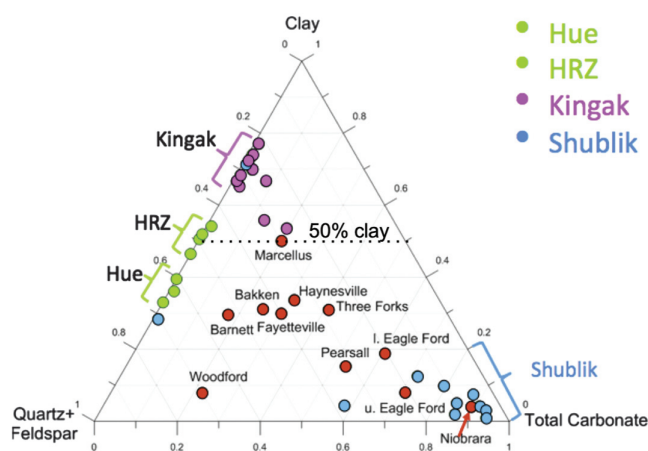


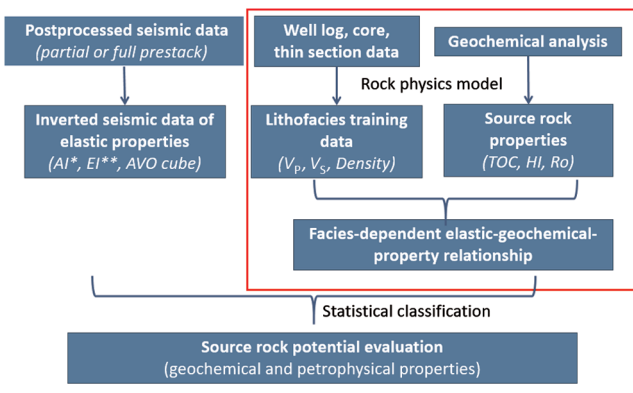
Figure 3. Ternary diagram of shale composition as a function of quartz, clay, and carbonate in weight fraction for the Shublik, Kingak, and Hue-HRZ source rocks in Alcor-1 and Merak-1 (Hosford et al., 2020). The pebble shale unit was not cored in those wells. The average compositions for Lower 48 shale plays are from Anderson (2014).

ment errors or borehole washout. Calibration of logging data based on available core data also is performed.

A challenge of this study is the lack of petrophysical and geochemical data in the same subset of core plugs because of different labs conducting experiments at different times. More broadly, well data alone cannot cover the whole dynamic spectrum of the variations in rock and fluid properties. Therefore, existing well-established workflows in the literature (i.e., Gassmann fluid substitution, lower Hashin-Shtrikman bounds, and Hertz-Mindlin [HM] contact theory) are used to fill the gaps or expand the available data set. We extend the HM values of the frame elastic moduli (for a given critical porosity) to all porosities by using the lower Hashin-Shtrikman bounds. Gassmann fluid substitution provides a means to calculate elastic moduli of different pore fluid saturations. In a single lithofacies, capturing the inherent variation of rock properties presents the most challenging aspect of QSI. This task becomes more difficult when a detected attribute difference implies a substantial change across multiple facies rather than a small internal fluctuation within a single facies (Avseth et al., 2005).

Data set

Two vertically oriented wells, Alcor-1 and Merak-1, were drilled south of the producing fields at the coast in 2012 (Figure 1). These wells, designed as stratigraphic tests for potential unconventional development, were cored extensively in the Hue, HRZ, Kingak, and Shublik intervals. In addition to the standard log suite, specialized logs include the dipole sonic log and spectral gamma-ray log. The two wells of interest are 1.5 miles (2.4 km) apart, and the penetrated units generally correlate well in their petrophysical properties and source rock character. Available core analyses include porosity, permeability, oil/gas saturation, XRD, and computed tomography scans. Also, geochemical data are available



* AI: Acoustic Impedance $AI = V_p * \text{Density}$
** EI: Elastic Impedance $EI = \text{Function}(V_p, V_s, \text{Density}, \text{Angle})$

Figure 4. Diagram showing the quantitative seismic interpretation workflow with the integration of geochemical data. In this study, we focus on the parts of the workflow that are related to the construction of a reliable elastic and geochemical training data set of each predefined lithofacies (shown inside the red rectangle).

for select core plug samples; these include TOC, programmed pyrolysis, and vitrinite reflectance. Geochemical measurements performed on well cuttings are excluded from the study. We sampled core plugs from Alcor-1 and Merak-1 to measure petrophysical and elastic properties with ultrasonic measurement devices. Sampling depths were chosen to be representative of each lithofacies (i.e., where each lithology visually appeared homogeneous and unfractured) and to cover a wide range of porosity, TOC, and lithology based on their logging signatures. Visible fractures and anomalous lithology (pyrite and bioturbation) were intentionally avoided. At each depth, if the bedding direction was clear, we sampled core plugs in three directions (bedding normal or vertical, bedding parallel or horizontal, and 45° to bedding), assuming that their depths were sufficiently close to representing similar lithology and texture. The results described in the rest of the paper focus on the vertically oriented core plugs.

Exploratory data analysis and seismic lithofacies definition

Logging data are used extensively in this study to build the representation of each seismic lithofacies in terms of elastic properties. Common logging tracks are plotted to verify several key signatures of each lithofacies (Figure 5). Except for the middle interval of the Hue Shale, the density of the remaining Hue Shale interval is comparable to the average density of the HRZ interval (Figure 5). However, the HRZ has a significantly higher gamma ray, as expected, and slightly lower sonic velocities compared to the upper interval of the overlying Hue Shale, attributed to smaller clastic dilution (more clay content) and less proximal deposition. A spike at 8700 ft (2652 m) in the density log in the Merak-1 well is due to a change in equipment after setting the intermediate casing. Therefore, the Hue Shale and HRZ will be separated into two separate lithofacies in the exploratory data analysis step. The pebble shale unit exhibits a wide range of density values due to the pebbles and well-rounded sand grains in its fine-grained matrix (Figure 5). In terms of radioactivity level and acoustic properties, Kingak Shale is a relatively homogeneous interval (Figure 5). In contrast, the density values of the Kingak Shale vary considerably. The Shublik Formation has intervals of abrupt high gamma-ray bands interbedded with lower gamma-ray intervals. Spikes in the gamma ray and density tracks indicate different amounts of clay and carbonate,

respectively, throughout the Shublik interval (Kupecz, 1995). It also has much higher P- and S-wave velocities compared to other facies because its matrix has a greater amount of carbonate (Avseth et al., 2005).

Crossplots of P- and S-wave velocities versus bulk density help distinguish North Slope shale units qualitatively. The Hue Shale and the HRZ display considerable fluctuations of acoustic velocity (V_P from 2800 to 4200 m/s in Alcor-1) within a small range of bulk density values (from 2.4 to 2.6 g/cm³) (the lower left panel in Figure 6). This trend is consistent in Merak-1 and Alcor-1, signifying possible trends in the regions between two wells. The pebble shale unit and the Kingak Shale exhibit relatively homogeneous shear velocities despite bulk density variation (from 1.7 to 2.6 g/cm³ in Merak-1) (the upper right panel in Figure 6). Lateral variability in lithofacies properties in the Merak-1 and Alcor-1 wells is demonstrated by comparing clusters from the same

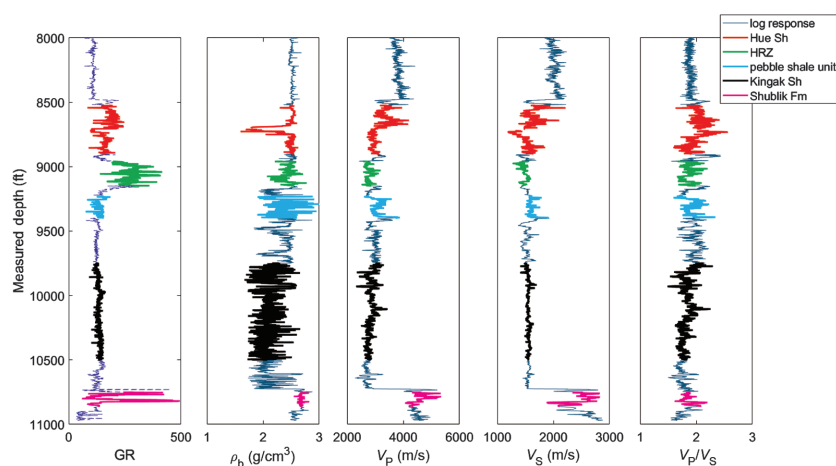


Figure 5. Diagram showing the log response of the organic-rich shales in the Merak-1 well. From top to bottom: Hue Shale (red), HRZ (green), pebble shale unit (blue), Kingak Shale (black), and Shublik Formation (pink). GR, gamma ray; g/cm³, grams per cubic centimeter. The geologic units are displayed with the same color code in Figures 7, 8, and 11. Fm, formation and Sh, shale.

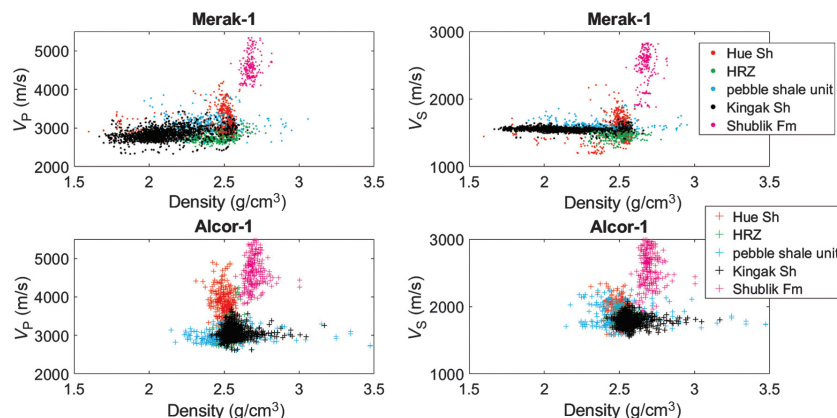


Figure 6. The V_P and V_S (m/s) versus bulk density (g/cm³) of the shale lithofacies in two wells: Merak-1 (top figures, the filled circles) and Alcor-1 (bottom figures, the colored plus signs). Fm, formation and Sh, shale.

lithofacies in two different wells (the upper versus lower panels in Figure 6). For example, this internal facies variability is noted by the absence of low-density components in the Kingak Shale and pebble shale unit Alcor-1 (Figure 6). The Shublik cluster is relatively unchanged in the two wells.

Another useful crossplot is V_P versus V_S (Figure 7). Shublik Formation and Hue Shale are readily distinguished from the other shale units by their relatively high sonic speeds. The Shublik Formation cluster yields the

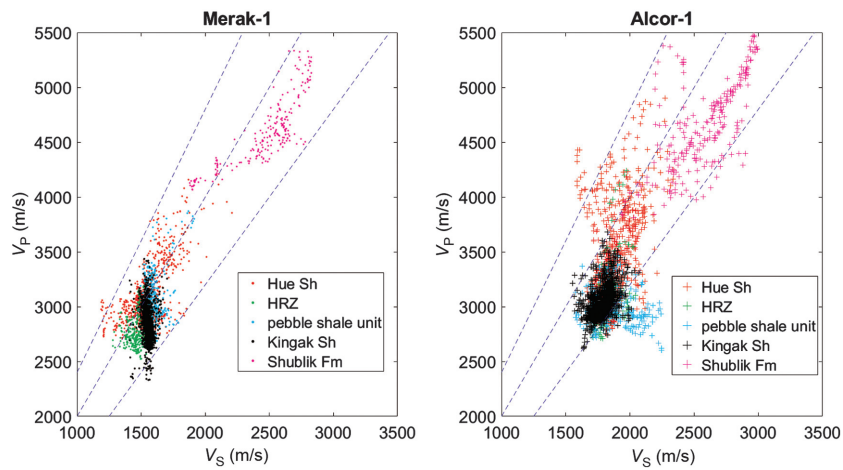


Figure 7. The V_S versus V_P from dipole sonic log in Merak-1 and Alcor-1. The blue dashed lines are the constant V_P/V_S ratio of 1.6, 2.0, and 2.4 (from the bottom to the top).

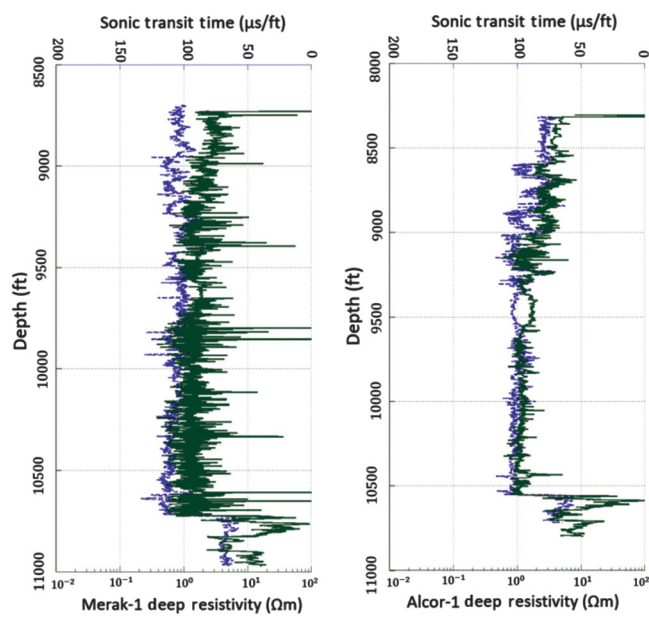


Figure 8. Superposition of deep resistivity and sonic transit time logs on a predefined scale (50 $\mu\text{m}/\text{ft}$ of sonic transit time to one resistivity cycle in log scale) shows good separation in the source rock intervals (Hue, Shublik, and Kingak) and moderate overlapping in the inorganic intervals. The blue curve is the sonic transit time ($\mu\text{m}/\text{ft}$), whereas the green curve is the deep resistivity (Ωm) in log scale. The left panel is Merak-1, and the right panel is Alcor-1.

highest sonic velocities (most $V_P > 4000$ m/s, most $V_S > 2200$ m/s). The Hue Shale is also recognizable due to its separation from other clusters (most $V_P > 3000$ m/s and most $V_S > 1800$ m/s). The V_P and V_S for the pebble shale unit, the Kingak Shale, and the HRZ exhibit similar sonic velocities (overlapping clouds in Figure 7) that are lower in magnitude than the Shublik Formation and Hue Shale units. The dashed blue lines represent lines of constant V_P/V_S with values of 1.6, 2.0, and 2.4 (from the bottom to top lines, respectively), which have been suggested to be a good indicator of organic-rich shale, with lower values of V_P/V_S than its non-organic counterparts (Vernik and Milovac, 2011).

In several published data sets compiled by Vernik and Milovac (2011) as well as in core and log data from the Bossier, Woodford, and Bakken shale plays, V_P/V_S data fall within a relatively narrow range regardless of the wide range of saturation, porosity, and effective stress. Thus, these parameters seem to be secondary to organic richness metrics in controlling the reduced V_P/V_S ratio compared to their inorganic counterpart. On the Alaska North Slope, the V_P/V_S ratio spans 1.6–2.4, a broader range compared to other shale plays, which generally span from 1.5 to 1.8 (Vernik and Milovac, 2011). The organically richer Shublik has the narrowest spread

and a lower average value of the V_P/V_S ratio compared to other lithofacies, which supports the inverse correlation suggested by Yan et al. (2012) between TOC content and V_P/V_S .

To bridge between geochemical and petrophysical data, densely spaced geochemical data are required downhole, ideally at the same depths as the petrophysical logs. Such coincident spacing is rarely if ever available; geochemical analyses are nearly always conducted at a sparser depth interval than log data. Thus, the computation of TOC from available logs, in this case, the resistivity log, is necessary to supplement the more sparsely distributed geochemical data. Resistivity measurements in logging devices are strongly dependent on thermal maturity because oil generation causes a rise in resistivity measurement whereas expelled gas (products of oil cracking at higher maturity) and thermally immature source rocks decrease resistivity (Mann et al., 1986). Low resistivity can therefore indicate either immature or overly matured or gas-only source rock. Hence, resistivity alone is not sufficient for TOC calculation. A common method to calculate TOC from logs is the $\Delta\log$ technique of Passey et al. (1990). The method involves overlaying a properly scaled porosity log or sonic transit time log on a resistivity curve (ideally from a deep resistivity tool) and subtracting them to obtain the TOC curve. Two major effects account for the difference between the two logging tracks: The presence of low-den-

sity, low-velocity kerogen deflects the transit time curve to higher values (lowering sonic velocity), whereas formation fluid in pore spaces deflects the resistivity curve to higher values. The generation and expulsion of petroleum from source rocks contribute to increasing resistivity in organic-rich intervals because of the replacement of electrically conductive pore water with nonconductive hydrocarbon.

In this study, superposition of deep resistivity and sonic transit time logs on a predefined scale (50 $\mu\text{m}/\text{ft}$ to one resistivity cycle in log scale) shows good separation in source rock intervals (Hue, Shublik, and Kingak) and moderate overlapping in inorganic intervals (Figure 8). The Miluvieach Sandstone is chosen as the baseline interval because the two curves are parallel and overlap in this interval. Values of baseline resistivity R_{baseline} and baseline transit time $\Delta t_{\text{baseline}}$, as well as resistivity and transit time of layers of interest, are used as inputs to calculate TOC (equation 1 from Passey et al., 1990):

$$\Delta \log R = \log\left(\frac{R}{R_{\text{baseline}}}\right) + 0.02 * (\Delta t - \Delta t_{\text{baseline}}) \quad (1)$$

$$\text{TOC} = \Delta \log R * 10^{2.297 - 0.1688 * \text{LOM}}, \quad (2)$$

where R and Δt are the measured resistivity and transit time in the organic interval, respectively, and LOM is the level of maturity as defined by Hood et al. (1975). Using this equation to solve for LOM, the thermal generation stage is determined for each source rock. For types II and III source rock, Passey et al. (1990) define the LOM value as the crossplot of programmed pyrolysis S2 peak versus TOC. For the Hue Shale (from Alcor-1) and the HRZ (from Merak-1), the LOM ranges from 6.5 to 9.5 (Figure 9). These values place the Hue-HRZ in the “main stage” to “advanced” hydrocarbon generation in the classification of Hood et al. (1975), consistent with programmed pyrolysis value of T_{max} in the nearby Toolik Federal-1 well (Peters et al., 2006). The Kingak Shale (from Merak-1) and Shublik Formation (from both wells) are in the “condensate and wet gas” hydrocarbon stage by the LOM of 12 (Figure 9), a stage that is corroborated by T_{max} in Toolik Federal-1 and Itkillik River-1 (Peters et al., 2006) and also with vitrinite reflectance data (Hosford Scheirer et al., 2017). The pebble shale unit does not have any core sampled for geochemical analysis.

Core analysis

P-wave and S-wave velocities extracted from sonic logs are plotted against bulk density from logs, dry core plugs, and as-received core plugs (Figure 10). The Shublik Formation shows a distinct separation because of high values in the bulk density and sonic velocities, which is consistent with Figure 6; thus, no correction between core and log values of bulk density is neces-

sary. However, other factors may obscure the value of the bulk density logs such as varying pyrite concentration and natural fracture systems. Log values of bulk density in the Kingak are lower than core values possibly due to the sampling bias of core plugs toward pyrite-free and unfractured intervals. The presence of heavy minerals, i.e., pyrite accounting for less than 10% in XRD analysis, was ignored for the sake of simplicity.

A simple correlation between geochemical and petrophysical parameters is not easy to make because the log response in shale intervals is complex and affected by not only the organics but also the mineralogical and pore fluid properties of rocks. Analyses of other shale plays (Bakken, Bazhenov, and Niobrara) compiled by Vernik and Milovac (2011) show that V_P increases as HI decreases, except in high-porosity shale in which V_P is better correlated with porosity (or density). Within a single lithofacies, the correlation is stronger, but it is not as significant as the velocity-density or V_P/V_S relationship (Figure 11). A statistically well-defined evaluation requires a comprehensive geochemical analysis of extensive core sets, which is time consuming and expensive. Because of possible wellbore integrity issues and organic mud additives, cuttings are not always reliable for determining subsurface lithology (Mann et al., 1986). Therefore, wireline log data, which offers a continuous profile of stratigraphic sections of interest with relatively high resolution, proves to be the best alternative. This is where the TOC logs established earlier are used. In the Shublik Formation, TOC and acoustic velocities form a distinct population with a weak linear trend in the velocity versus TOC crossplot (Figure 11). Data from the Hue Shale and the HRZ cluster in the wavespeed-TOC space, with a limited wave velocity spread (2500–3500 m/s for V_P and 1400–1600 m/s for V_S) over a wide range of organic carbon content (0–10 wt%). The pebble shale and the Kingak Shale also overlap at about the same P-wave and S-wave values but over a narrower TOC range (0–4 wt%) than the Hue/HRZ (Figure 11).

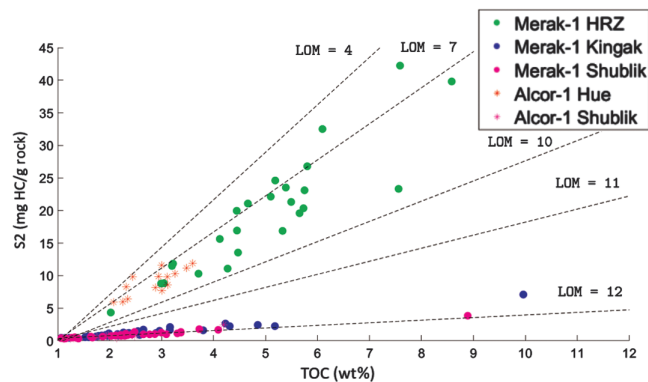


Figure 9. The S2 in mg hydrocarbon/g rock versus TOC (wt %) of core plugs in the geochemical data set. The black lines are the LOM as defined by Passey et al. (1990).

Rock physics template

Rock physics models link seismic properties to geologic properties (Avseth et al., 2005; Mavko et al., 2020).

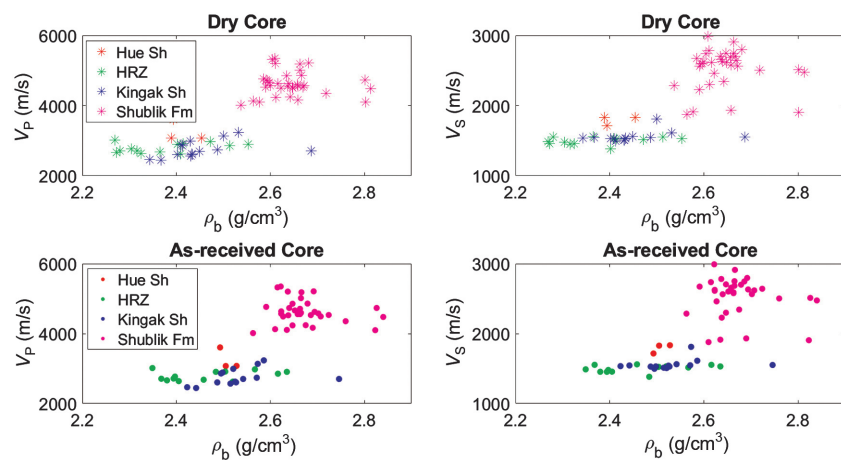


Figure 10. The P- and S-wave velocities (m/s) versus bulk density (gm/cm^3). The top images are for the dry core (the asterisk), whereas the bottom images are for the as-received cores (the filled circles). The saturation of the as-received core does not significantly change the bulk density because North Slope shale units have low porosity. The density log values of the Kingak Shale are lower than the core values possibly due to the sampling bias of core plugs toward pyrite-free and unfractured intervals.

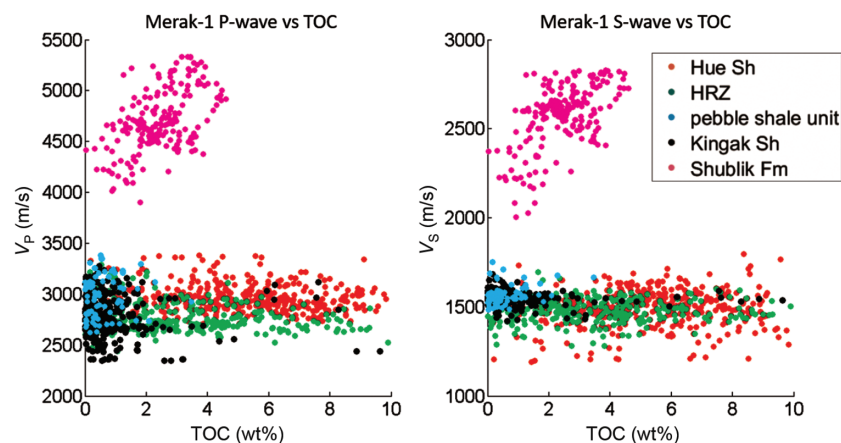


Figure 11. The P- and S-wave velocities versus the log-derived TOC values for Merak-1. The TOC and acoustic velocities exhibit a positive correlation in the Shublik Formation, whereas no correlation exists between the other shale units.

Table 1. Simplified composition for HRZ, Kingak, and Shublik used as inputs for the soft sediment rock-physics model. Data are from core analysis of Merak-1 and Alcor-1 samples. Composition data are unavailable for the Hue Shale and the pebble shale unit.

	Illite (%)	Calcite (%)	Quartz (%)	Kerogen (%)
HRZ	30	0	40	30
Kingak	30	0	50	20
Shublik	5	35	40	20

Expanding on the earlier exploratory data analysis and diagnostics, we create an RPT for each lithofacies using two selected seismic parameters, acoustic impedance (AI, which is the product of bulk density and P-wave velocity) and V_P/V_S ratio. Geologic trends (pressure variation, pore fluid, sorting, and cementation) also play a role in constraining rock physics models. By modeling the variation of seismic-derived attributes (AI and V_P/V_S) as a function of depositional trend or burial history, we can predict the lithology, porosity, density, and fluid content of un-drilled regions, pinpointing sweet spots for development drilling (Avseth et al., 2005). The RPT allows a rock physics analysis not only on well-log data but also on the results of elastic inversion of seismic data.

Data on mineralogy is derived from XRD measurements; these are available in Alcor-1 for the HRZ, the Kingak Shale, and the Shublik Formation (Table 1). To simplify the matrix composition, only minerals that constitute critical inputs in rock physics modeling — quartz, clay (mainly illite), and carbonate — are considered. Note that pyrite is prevalent in core plugs from the HRZ, comprising approximately 10% by volume, but pyrite is excluded here for the sake of simplicity. Table 1 presents the simplified lithology of the HRZ, Kingak, and Shublik intervals; these will be used to establish a rock physics soft-sediment template for these units. Other inputs of the soft-sediment model are the mineral and fluid bulk/shear modulus (Table 2). The soft-sediment model (Dvorkin and Nur, 1996; Mavko et al., 2020) uses HM contact theory (Mindlin, 1949) to calculate the elastic moduli of high-porosity end members at critical porosity and the modified lower Hashin-Shtrikman bound (Hashin and Shtrikman, 1963) to interpolate to the low-porosity end members.

The zero-porosity end member is a pure mineral mix of quartz, clay, and calcite, assuming that other minerals appear as only trace amounts in the matrix composition. The RPT used here requires several inputs (effective pressure and volume composition) to calculate the shale elastic properties (acoustic velocities at different saturations, bulk density). Pressure data are limited in Alcor-1 and Merak-1, so as a working assumption, standard lithostatic and pore pressure gradients are assumed (1 and 0.433 psi/ft, respectively) for calculation of the effective pressure. Although organic shale formations can be significantly overpressured, one DFIT measurement in Alcor-1 showed only mild

overpressure in the Shublik Formation at these depths. Therefore, the effective pressure gradient is assumed to be 0.567 psi/ft, which is the difference between standard lithostatic and pore-pressure gradients. Other inputs of the soft-sediment model are the mineral and fluid bulk/shear modulus and critical porosity; the latter is 0.7 for shale (Mavko et al., 2020).

The RPT model calculates shale elastic moduli from which V_P/V_S versus P-wave impedance trends are superimposed on log-derived data points. The soft-sediment model examines the expected changes of these seismic attributes concerning changes in pore fluid, pressure, clay content, and mineralogy (the arrows in Figures 12, 13, and 14). This step also serves as a checkpoint to ensure log quality because trends of bulk density variation should match the trend of shale density magnitude. The crossplot of AI versus V_P/V_S reveals the trend of RPT-related property change due to shaliness/clay content in the Hue/HRZ (arrow 2 in Figure 12). The Hue Shale and HRZ are grouped in the RPT construction because the radioactivity difference was found not to have a large impact on elastic properties. A rock physics model is not developed for the pebble shale unit

Table 2. Elastic moduli of different minerals (Avseth et al., 2005). Alaska North Slope kerogen elastic properties are limited, so we use typical values of kerogen modulus and density at similar maturity level from other shale plays (Vernik and Milovac, 2011).

Clay mineral	Bulk Modulus K (GPa)	Shear Modulus μ (GPa)	Density Rho (g/cm^3)
Quartz	36.6	45	2.65
Illite	39.4	11.7	2.75
Calcite	76.8	32	2.71
Kerogen	6.8	3.6	1.40

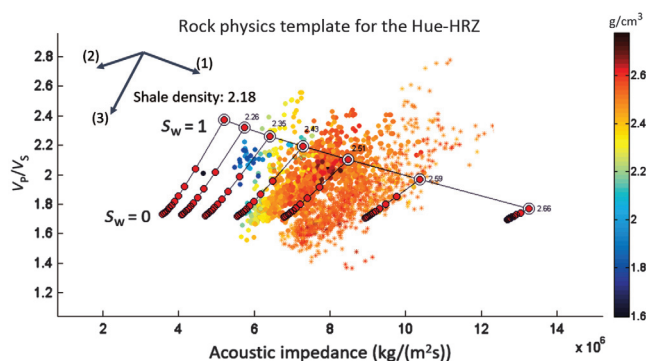


Figure 12. RPT of the Hue and HRZ interval presented as crossplots of V_P/V_S versus AI. This includes a rock-physics model locally constrained by depth (i.e., pressure), mineralogy, critical porosity, and fluid properties. The arrows indicate conceptual geologic trends: (1) decreasing porosity (or increasing bulk density), (2) increasing shale content, and (3) increasing gas saturation.

because of its observed independency of AI on the V_P/V_S ratio in the exploratory data analysis. The branching skeleton in Figures 12, 13, and 14 represents the expected change during pore fluid substitution as gas displaces water in pore spaces (S_w varies from 0 to 1). Here, we use the standard Gassmann equations (Gassmann, 1951; Mavko et al., 2020) for fluid substitution. Strictly speaking, the standard fluid substitution recipe has to be used with caution because the shale lithology defies the assumptions of Gassmann's formula due to the presence of bound water in clays (Smith et al., 2003).

The input parameters of the forward rock physics model are obtained by matching the elastic properties derived from the well logs against those generated from the forward rock physics modeling. By adjusting the input dry bulk and shear moduli, the soft-sediment model reasonably matches the bulk density of low-porosity (or

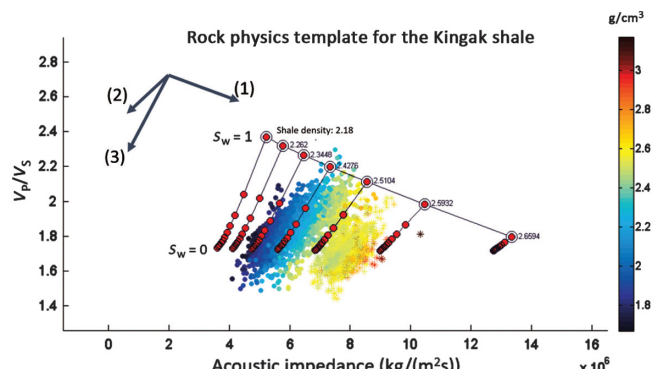


Figure 13. RPT of the Kingak Shale presented as crossplots of V_P/V_S versus AI. The template includes porosity trends for different fluid saturation (from fully water saturated $S_w = 1$ to fully gas saturated $S_w = 0$) assuming uniform saturation. The color bar indicates the range of bulk density (g/cm^3). The arrows indicate conceptual geologic trends: (1) decreasing porosity (or increasing bulk density), (2) increasing shale content, and (3) increasing gas saturation.

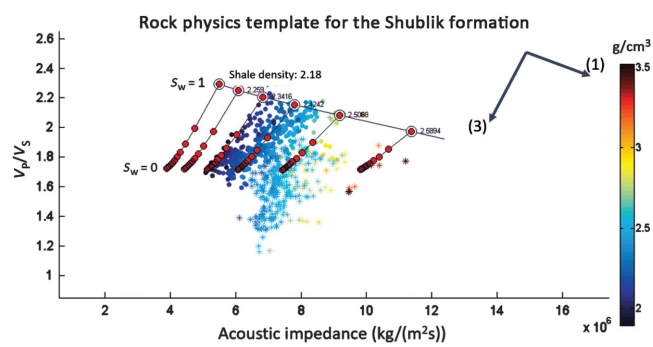


Figure 14. RPT of the Shublik Formation presented as crossplots of V_P/V_S versus AI. The template includes porosity trends for different fluid saturation (from fully water saturated $S_w = 1$ to fully gas saturated $S_w = 0$) assuming uniform saturation. The color bar indicates the range of bulk density (g/cm^3). The arrows indicate conceptual geologic trends: (1) decreasing porosity (or increasing bulk density), (2) increasing shale content, and (3) increasing gas saturation.

high-density) members. Despite the inclusion of low-density kerogen in the model, low-density members (the blue points in Figures 12, 13, and 14) are not exactly matched; they fall into a higher density zone. This is likely because the soft-sediment model does not account for an effective pressure anomaly within the interval. The effects of organic content and hydrocarbon-filled pore space may be the cause of scattering deviation in the clusters of each lithofacies away from the main trend lines. Additionally, the rock physics model itself is imperfect. The high-porosity endpoint is assumed to be well described by the HM elastic contact theory, which is based on the behavior of an elastic sphere subject to confining pressure. This is more applicable to sand, or to some extent shaly sand, than to the shale facies that we model here (Avseth et al., 2005); any rock physics model has assumptions that are violated by real rocks and hence always require calibration. However, a calibrated HM model when combined with the modified lower bound Hashin-Shtrikman serves as a heuristic model to describe velocity-porosity trends for rocks that have high clay content (Avseth et al., 2005). Another explanation for the misfit of the low-density members could be that the logging device was responding to a layer of low-density organic material but not necessarily the shale matrix. To better fit the bulk density of high-porosity (or low-bulk-density) components, inputs to the rock physics model — shear reduction factor, coordination number in the HM model, kerogen composition, and petrophysical properties — are modified (Tran, 2014).

As discussed earlier, the Hue Shale and HRZ are separated in the exploratory data analysis. In this section, these two will be combined into one template because, based on the crossplots between GR and sonic velocity, the radioactivity level does not have much correlation with the elastic properties. The RPT for the Hue-HRZ interval is shown in Figure 12. Three conceptual geologic directional trends are embedded in the template, as shown by the numbered arrows: (1) decreasing porosity (or increasing bulk density), (2) increasing shale content, and (3) increasing gas saturation. The Hue/HRZ cluster covers the whole spectrum of fluid saturations, which implies that the template can capture the large variation in fluid type and saturation level. The effects of assumed fluids on acoustic properties are problematic because shale lithology defies the main assumptions of Gassmann theory (typically used for clean sandstone) due to rock (clay)-fluid interaction and due to overpressure caused by low permeability. Gassmann fluid substitution is limited to interchangeable substitution of two fluids (in this case, water and gas). The predicted saturation of the soft-sediment model overestimates to a small degree the gas saturation compared to wet core plugs (at the corresponding log depths). This is most likely due to gas being inadequately preserved in core plugs or due to the omission of oil in the fluid substitution recipe in the soft-sand model.

There are several challenges in modeling the composition of organic-rich shale and the effects of porosity

on velocity. Porosity is not easily determined from log data due to the heterogeneous lithology and ambiguity in measurement accuracies, such as neutron tools in the log suite or ultra-low-permeability plugs. Therefore, the bulk density is used instead of porosity in the RPTs. Figure 13 shows the RPT for the Kingak Shale, in which density appears to be the principal driving force of the V_P/V_S — AI trend because it shows a clear gradational trend when similar color-filled circles are lining up properly in each branching skeleton. The expanded log data does not cover the extreme ends of low and high porosity as expected because log data represent an actual geologic rock unit compared to the template's endpoints, which represent the theoretical limit of the underlying rock physics assumptions. The Kingak cluster does not exhibit scattering behavior above the skeleton compared to the Hue/HRZ cluster, proving that the model better captures the internal variation of elastic behavior within the Kingak Shale (Figure 13).

The adjustment of model parameters for each template is different to ensure a proper fit for the log data. The rock physics model for the Shublik Formation shows some high-density data in the lower density range, probably because high-density pyrite is ignored in the model (Figure 14). Additionally, there are clusters of southernmost points stretching below the skeleton, which suggests that the mineralogy composition of Shublik in the model needs further refinements. This can be validated by performing additional measurements on actual core plugs to adjust the mineral composition input to the template.

Conclusion

Major shale seismic lithofacies in the North Slope, Alaska, can be qualitatively delineated in terms of multivariate distributions of their elastic and petrophysical properties using exploratory data analysis and rock-physics diagnostics. Crossplots between the elastic properties, petrophysical properties, and geochemical properties show some degrees of separation among different shales, especially for the Shublik Formation with a relatively strong correlation between TOC and the sonic velocities observed. The Hue Shale and HRZ can be separated in the V_P versus V_S crossplot with a good degree of separation, whereas the Kingak Shale and pebble shale units usually have significant overlap in most crossplots. There is a complex synergy of various factors dictating the behavior of velocity-density trend for each lithofacies: organic material, clay content, mineralogy, pressure, temperature, and fluid properties, of which their degrees of contribution are strongly facies-dependent. Existing shale petrophysical models can be reasonably applied to organic-rich shales provided that they are calibrated to the regional geology of the sedimentary basin of consideration. The soft-sediment model is applied to produce RPTs, which result in good agreement for bulk density, especially for high-density constituents. These templates show how various geologic trends (pressure, saturation, clay content, and mineralogy) affect seis-

mic-related attributes (AI and V_P/V_S ratio). These locally calibrated templates will aid in the evaluation of undrilled regions in terms of elastic and source rock properties based on the seismic inversion signature, thus facilitating identification of the next sweet spots to drill and develop in North Slope Alaska.

Acknowledgments

We thank Great Bear Petroleum for providing the data set for this study prior to its public release. We thank K. Bird and L. Magoon for their insightful comments. Funding was provided from the Basin and Petroleum System Modeling (BPSM) and Stanford Center for Earth Resources Forecasting (SCERF) industrial affiliates programs.

Data and materials availability

Data associated with this research are available and can be obtained by contacting the corresponding author.

References

- Anderson, T., 2014, Parameters for liquid-rich unconventional plays: Case studies from North America: Presented at the AAPG Geoscience Technology Workshop.
- Avseth, P., T. Mukerji, and G. Mavko, 2005, Quantitative seismic interpretation: Applying rock physics tools to reduce interpretation risk: Cambridge University Press.
- Bhattacharya, S., and R. C. Timothy, 2019, Integrated data-driven 3D shale lithofacies modeling of the Bakken Formation in the Williston Basin, North Dakota, United States: *Journal of Petroleum Science and Engineering*, **177**, 1072–1086, doi: [10.1016/j.petrol.2019.02.036](https://doi.org/10.1016/j.petrol.2019.02.036).
- Bird, K. J., 1994, Ellesmerian(!) petroleum system, North Slope of Alaska, U.S.A., in L. B. Magoon and W. G. Dow, eds., *The petroleum system — From source to trap*: AAPG Memoir **60**, 339–358.
- Bird, K. J., 2001, Alaska: A twenty-first-century petroleum province, in M. W. Downey, J. C. Threet, and W. A. Morgan, eds., *Petroleum provinces of the twenty-first century*: AAPG Memoir **74**, 137–165.
- Dvorkin, J., and A. Nur, 1996, Elasticity for high-porosity sandstones: Theory for two North Sea datasets: *Geophysics*, **61**, 1363–1370, doi: [10.1190/1.1444059](https://doi.org/10.1190/1.1444059).
- Gassmann, F., 1951, Elasticity of porous media: *Vierteljahrsschrder Naturforschenden Gesellschaft*, **96**, 1–23.
- Gupta, N., C. S. Rai, and C. H. Sondergeld, 2013, Petrophysical characterization of the Woodford shale: *Petrophysics*, **54**, 368–382.
- Hashin, Z., and S. Shtrikman, 1963, A variational approach to the elastic behavior of multiphase materials: *Journal of the Mechanics and Physics of Solids*, **11**, 127–140, doi: [10.1016/0022-5096\(63\)90060-7](https://doi.org/10.1016/0022-5096(63)90060-7).
- Hood, A., C. C. M. Gutjahr, and R. L. Heacock, 1975, Organic metamorphism and the generation of petroleum: *AAPG Bulletin*, **59**, 986–996, doi: [10.1306/83D91F06-16C7-11D7-8645000102C1865D](https://doi.org/10.1306/83D91F06-16C7-11D7-8645000102C1865D).
- Hosford Scheirer, A., and K. J. Bird, 2020, A lateral well in the Shublik Formation, Alaska North Slope, with implications for development of unconventional resource potential: *Interpretation*, **8**, no. 2, SJ35–SJ49, doi: [10.1190/INT-2019-0186.1](https://doi.org/10.1190/INT-2019-0186.1).
- Hosford Scheirer, A., L. B. Magoon, K. J. Bird, and E. A. Duncan, 2017, Evaluating the Shublik Formation as an unconventional resource play on the Alaska North Slope: Presented at the Unconventional Resources Technology Conference, AAPG, doi: [10.15530/URTEC-2017-2697424](https://doi.org/10.15530/URTEC-2017-2697424).
- Houseknecht, D. W., and K. J. Bird, 2006, Oil and gas resources of the Arctic Alaska petroleum province, in P. J. Haeussler and J. P. Galloway, eds., *Studies by the U.S. Geological Survey in Alaska, 2005: U.S. Geological Survey Professional Paper 1732*, 1–11, <https://pubs.usgs.gov/pp/pp1732/pp1732a/>, accessed 12 March 2020.
- Hubbard, R. J., S. P. Edrich, and R. P. Rattey, 1987, Geologic evolution and hydrocarbon habitat of the ‘Arctic Alaska microplate’: *Marine and Petroleum Geology*, **4**, 2–34, doi: [10.1016/0264-8172\(87\)90019-5](https://doi.org/10.1016/0264-8172(87)90019-5).
- Keller, M. A., and J. H. S. Macquaker, 2001, High resolution analysis of petroleum source potential and lithofacies of Lower Cretaceous mudstone core (Pebble shale unit and GRZ of Hue Shale), Mikkelsen Bay State #1 well, North Slope Alaska: Presented at the NPRA SPEM Core Workshop 21, 37–56.
- Kupecz, J. A., 1995, Depositional setting, sequence stratigraphy, diagenesis, and reservoir potential of a mixed lithology, upwelling deposit: Upper Triassic Shublik Formation, Prudhoe Bay, Alaska: *AAPG Bulletin*, **79**, 1301–1319, doi: [10.1306/7834D4AE-1721-11D7-8645000102C1865D](https://doi.org/10.1306/7834D4AE-1721-11D7-8645000102C1865D).
- Lease, R. O., D. W. Houseknecht, A. R. Kylander-Clark, K. J. Whidden, and J. A. Dumoulin, 2018, Cretaceous foreland dynamics, eustasy, and climate from continental shelf and distal sections, Arctic Alaska: Fall Meeting, American Geophysical Union.
- Magoon, L. B., and K. J. Bird, 1985, Alaskan North Slope petroleum geochemistry for the Shublik Formation, Kingak Shale, pebble shale unit, and Torok Formation, in L. B. Magoon and G. E. Claypool, eds., *Alaska North Slope oil/source rock correlation study: AAPG Studies in Geology* **20**, pp. 31–48.
- Magoon, L. B., and G. E. Claypool, 1984, The Kingak Shale of north Alaska — Regional variations in organic geochemical properties and petroleum source rock quality: *Organic Geochemistry*, **6**, 533–542, doi: [10.1016/0146-6380\(84\)90076-7](https://doi.org/10.1016/0146-6380(84)90076-7).
- Magoon, L. B., P. G. Lillis, K. J. Bird, C. Lampe, and K. E. Peters, 2003, Alaskan North Slope petroleum systems: U.S. Geological Survey Open-File Report 03-324, <https://doi.org/10.3133/ofr2003324>, accessed 12 February 2020.
- Mann, U., D. Leythaeuser, and P. J. Muller, 1986, Relation between source rock properties and wireline log parameters: An example from Lower Jurassic Posidonia Shale, NW-Germany: *Advances in Organic Geochemistry*, **10**, 1105–1112, doi: [10.1016/S0146-6380\(86\)80051-1](https://doi.org/10.1016/S0146-6380(86)80051-1).
- Mavko, G., T. Mukerji, and J. Dvorkin, 2020, *The rock physics handbook*, 3rd ed.: Cambridge University Press.

- Mindlin, R. D., 1949, Compliance of elastic bodies in contact: *Journal of Applied Mechanics*, **16**, 259–268, doi: [10.1007/978-1-4613-8865-4_24](https://doi.org/10.1007/978-1-4613-8865-4_24).
- Molenaar, C. M., K. J. Bird, and A. R. Kirk, 1987, Cretaceous and tertiary stratigraphy of northeastern Alaska: Alaskan North Slope Geology, **1**, 513–528.
- Parrish, J. T., 1987, Lithology, geochemistry, and depositional environment of the Shublik Formation (Triassic), northern Alaska, in I. L. Tailleur and P. Weimer, eds., *Alaskan North Slope geology: Pacific Section Society for Sedimentary Geology*, 391–396.
- Passey, Q. R., S. Creaney, J. B. Kulla, F. J. Moretti, and J. D. Stroud, 1990, A practical model for organic richness from porosity and resistivity logs: *AAPG Bulletin*, **74**, 1777–1794, doi: [10.1306/0C9B25C9-1710-11D7-8645000102C1865D](https://doi.org/10.1306/0C9B25C9-1710-11D7-8645000102C1865D).
- Peters, K. E., and M. R. Cassa, 1994, Applied source rock geochemistry, in L. B. Magoon and W. G. Dow, eds., *The petroleum system — From source to trap: AAPG Memoir* **60**, pp. 93–120.
- Peters, K. E., L. B. Magoon, K. J. Bird, Z. C. Valin, and M. A. Keller, 2006, North Slope, Alaska — Source rock distribution, richness, thermal maturity, and petroleum charge: *AAPG Bulletin*, **90**, 261–292, doi: [10.1306/09210505095](https://doi.org/10.1306/09210505095).
- Peters, K. E., L. S. Ramos, J. E. Zumberge, Z. C. Valin, and K. J. Bird, 2008, De-convoluting mixed crude oil in Prudhoe Bay Field, North Slope, Alaska: *Organic Geochemistry*, **39**, 623–645, doi: [10.1016/j.orggeochem.2008.03.001](https://doi.org/10.1016/j.orggeochem.2008.03.001).
- Robison, V. D., L. M. Liro, C. R. Robison, W. C. Dawson, and J. W. Russo, 1996, Integrated geochemistry, organic petrology, and sequence stratigraphy of the Triassic Shublik Formation, Tenneco Phoenix #1 well, North Slope, Alaska: *Organic Geochemistry*, **24**, 257–272, doi: [10.1016/0146-6380\(96\)00023-X](https://doi.org/10.1016/0146-6380(96)00023-X).
- Saneifar, M., R. Conte, C. C. Valdes, Z. Heidari, and M. C. Pope, 2015, Integrated rock classification in carbonate formations based on elastic and petrophysical properties estimated from conventional well logs: *AAPG Bulletin*, **99**, 1261–1280, doi: [10.1306/02091514167](https://doi.org/10.1306/02091514167).
- Smith, T. M., C. H. Sondergeld, and C. S. Rai, 2003, Gassmann fluid substitutions: A tutorial: *Geophysics*, **68**, 430–440, doi: [10.1190/1.1567211](https://doi.org/10.1190/1.1567211).
- Temizel, C., H. Kirmaci, Z. Wijaya, K. Balaji, A. Suhag, R. Ranjith, M. Tran, B. Al-Otaibi, A. Al-Kouh, Y. Zhu, and C. Yegin, 2016, Production optimization through voidage replacement using triggers for production rate: Heavy Oil Conference and Exhibition, SPE.
- Tran, M., F. Aminzadeh, and B. Jha, 2018, Effect of coupled flow and geomechanics on transport of a fluid slug in a stress-sensitive reservoir: 52nd US Rock Mechanics/Geomechanics Symposium, American Rock Mechanics Association.
- Tran, M., and B. Jha, 2020, Coupling between transport and geomechanics affects solute spreading and mixing during viscous fingering in deformable aquifers: *Advances in Water Resources*, **136**, 103485, doi: [10.1016/j.advwatres.2019.103485](https://doi.org/10.1016/j.advwatres.2019.103485).
- Tran, M. T., 2014, Formation evaluation of an unconventional shale reservoir: Application to the North Slope Alaska: M.S. thesis, Stanford University.
- Vernik, L., and J. Milovac, 2011, Rock physics of organic shales: *The Leading Edge*, **30**, 318–323, doi: [10.1190/1.3567263](https://doi.org/10.1190/1.3567263).
- Yan, F., D. Han, and Q. Yao, 2012, Oil shale anisotropy measurement and sensitivity analysis: 82nd Annual International Meeting, SEG, Expanded Abstracts, doi: [10.1190/segam2012-1106.1](https://doi.org/10.1190/segam2012-1106.1).
- Yurchenko, I. A., J. M. Moldowan, K. E. Peters, L. B. Magoon, and S. A. Graham, 2018, Source rock heterogeneity and migrated hydrocarbons in the Triassic Shublik Formation and their implication for unconventional resource evaluation in Arctic Alaska: *Marine and Petroleum Geology*, **92**, 932–952, doi: [10.1016/j.marpetgeo.2018.03.033](https://doi.org/10.1016/j.marpetgeo.2018.03.033).



Minh Tran received a B.S. (2012) degree, summa cum laude, in petroleum engineering with a minor in geology at the University of Oklahoma, Norman, OK, USA. He received an M.S. degree (2014) in petroleum engineering at Stanford University, Stanford, California, USA. He completed his master's thesis titled "Formation evaluation of an unconventional shale reservoir: Application to the North Slope Alaska." He worked as a production engineer at Belridge and Lost Hills oil fields for Aera Energy LLC (Bakersfield, CA, USA) from 2014 to 2015. After that, he served as a reservoir engineer for PetroVietnam between 2015 and 2016, working in the block B multinational project in the Gulf of Thailand. Currently, under a full provost fellowship funding, he is a Ph.D. candidate in petroleum engineering and a master's in computer science at the University of Southern California, Los Angeles, CA, USA. His research interest focuses on numerical simulation of enhanced oil recovery and CO₂ sequestration processes in fractured porous media through an integrated workflow coupling flow, transport, geomechanics, and phase field modeling. His research interest also includes applications of machine learning and big data mining in oil and gas applications.



Tapan Mukerji is a professor (research) in the Department of Energy Resources Engineering. He codirects the Stanford Center for Earth Resources Forecasting, the Stanford Rock Physics and Borehole Geophysics, and the Stanford Basin and Petroleum System Modeling research groups. Tapan obtained his Ph.D. (1995) in geophysics from Stanford University and M.S. (geophysics) and B.S. (physics) degrees from Banaras Hindu University, India. His research interests include rock physics, spatial statistics, wave propagation, stochastic methods for quantitative reservoir characterization, time-lapse reservoir

monitoring, geomodeling, and value of information applications in geosciences. He was awarded the Karcher Award in 2000 by SEG. He is a coauthor of *The Rock Physics Handbook*, *Quantitative Seismic Interpretation*, and *The Value of Information in the Earth Sciences* — all published by Cambridge University Press. In 2014, Tapan (together with G. Mavko, J. Dvorkin, and D. Grana) was awarded the ENI award — the so-called Energy Nobel Prize — for pioneering innovations in theoretical and practical rock physics for seismic reservoir characterization. In 2017, Tapan's book *The Value of Information in the Earth Sciences* received the finalist publication competition award from the Decision Analysis Society of the Institute for Operations Research and Management Sciences.



Allegra Hosford Scheirer is a research scientist at Stanford University, where she is a principal scientist in the Basin and Petroleum System Modeling Industrial Affiliates Program, teaches graduate level courses, and advises graduate students and postdoctoral scholars. Prior to Stanford, Allegra was a member of the Geophysical Unit of Menlo Park and the Energy Resource Program at the U.S. Geological Survey. She is the editor of USGS Professional Paper 1713 and a past associate editor of the *Journal of Geophysical Research*. Allegra's degrees are from the MIT-WHOI Joint Program in Oceanography (Ph.D.) and Brown University (geology-physics/math).